JOURNAL OF COLLOID AND INTERFACE SCIENCE 167, 66–73 (1994)

Capillary Image Forces

II. Experiment

ORLIN D. VELEV,* NIKOLAI D. DENKOV,* VESSELIN N. PAUNOV,*
PETER A. KRALCHEVSKY,*,[1] AND KUNIAKI NAGAYAMA†

* *Laboratory of Thermodynamics and Physicochemical Hydrodynamics, Faculty of Chemistry, University of Sofia, 1126 Sofia, Bulgaria; and † Protein Array Project, ERATO, JRDC, 5-9-1 Tokodai, Tsukuba, 300-26 Japan*

Received November 1, 1993; accepted March 8, 1994

The capillary meniscus interaction between a floating submillimeter particle and a vertical wall is experimentally studied. It is proven that the interplay of the capillary image force from one side and the gravity and buoyancy forces from the other side can lead to the appearance of a stable equilibrium position of the particle at a finite distance from the wall. The dependence of the equilibrium separation on the particle size, three-phase contact angle, and other parameters is investigated and compared with the theory developed in the first part of this study. The agreement between the experimental results and the theoretical predictions is very good. A simple method for determination of the three-phase contact angle of millimeter- and submillimeter-size particles, floating attached to a fluid interface, is described.

1. INTRODUCTION

The lateral capillary forces acting between bodies attached to a fluid interface have been the subject of many theoretical studies (1–11). In contrast, there are only a few studies where these forces have been measured experimentally (2, 11, 12). Gifford and Scriven (2) reported the qualitative features of the interaction between two long cylindrical capillaries floating on a water surface (the cylinder axes being parallel to the surface). Camoin *et al.* (12) measured directly the capillary force between two plastic spheres of millimeter size attached to vertical holders. These authors showed that the lateral capillary force decays approximately exponentially with the particle separation. They investigated also the magnitude of the capillary force as a function of the vertical position of the particles (controlled by the holders) with respect to the fluid surface. The lack of information about some important parameters (interfacial tension and three-phase contact angle) in Ref. (12) does not allow direct comparison of the experimental results with the theory. Another feature of these experiments is that the spheres are attached to vertical holders, so their vertical positions are kept constant when the interparticle separation is varied. Hence, an *immersion*-type lateral capillary force (6, 8) was measured. It should be distinguished from the *flotation*-type lateral capillary force which appears between freely floating spheres of millimeter and submillimeter size and is governed mainly by the gravitational energy of the particles due to the change in their vertical position (1, 3, 6).

In Ref. (11) immersion-type lateral capillary forces between two vertical capillaries, or between a vertical capillary and a wall, were directly measured and compared with the theory. Both attractive forces (between two hydrophilic bodies) and repulsive forces (between a hydrophilic and a hydrophobic body) were studied. The agreement between the experimental results and the theoretical predictions was very good. As discussed in Refs. (4, 5, 11) the interaction between two vertical cylinders models the one between two spheres of fixed "capillary charge" as defined in Eq. [2.6] in the first part of this study (13).

One can conclude from this brief literature review that until now there has been no quantitative experimental study of flotation-type lateral capillary forces, i.e., forces acting between *floating* bodies.

In the first part of this study (13) we studied theoretically the capillary interaction between a floating spherical particle and a wall. It is established that analogously to electrostatics the particle–wall interaction is similar to the interaction of the particle with its mirror image with respect to the wall. This *capillary image force* can be *attractive* when the contact angle at the wall is constant, or *repulsive* when the position of the contact line at the wall is fixed. The total capillary interaction includes (along with the capillary image force) the contributions of the particle weight and the upthrust. It is shown that at certain parameters of the system the total capillary interaction energy has a minimum as a function of the interparticle separation. In such case the particle acquires a stable equilibrium position at a certain distance from the wall. At this distance the repulsive capillary image force

[1] To whom correspondence should be addressed.

0021-9797/94 $6.00

(which prevails at small separations) exactly counterbalances the effective attractive net force due to the combination of weight and upthrust. This theoretical prediction suggests an experiment for verification of the derived expressions for the lateral capillary forces by direct measurement of the equilibrium particle–wall separation as a function of some appropriate parameter.

The main goal of this study is the verification of the theory of the capillary image forces against experimental results. As shown below, the agreement between the theory and experiment is very good. Since the capillary image force is equivalent to the interaction between two floating spheres (the particle and its mirror image), the results obtained represent not only the particle–wall interaction but also the interaction of two floating particles. In addition, a simple and precise method for determination of the three-phase contact angle of floating spherical particles of millimeter and submillimeter size is formulated.

The article is organized as follows: in Section 2 we describe the methods and materials used, in Sections 3 and 4 the procedures for calculating the particle three-phase contact angle and the theoretical curves are outlined, and in Section 5 the experimental results are presented and compared with the theory. The conclusions are summarized in Section 6. The notations are the same as in the first part of this study (13).

2. EXPERIMENTAL

(a) Materials

The experiments were performed on the surface of pure water extracted from a Millipore Milli-Q Organex system. Surface tension measurements of the water have determined a value of 72.0 ± 0.3 mN/m. Before the measurements were performed, the liquid surface was additionally cleaned by sucking with glass pipette.

Two types of particles floating on the water surface were studied. The first type was drops from high-purity (6N grade) mercury produced by Mitsuwa's Pure Chemicals (Japan). The second type of particle was copper beads of millimeter size (Stanley Co., Japan).

The glass vessel holding the liquid, the Teflon barrier, and the instrumental glassware were cleaned by immersion in chromic acid for not less than 24 h, followed by abundant washing with deionized water and vacuum drying.

(b) Methods

A schematic description of the experimental setup is presented in Fig. 1. The particle (1) floats on the water surface (3). The water is poured inside a wide glass dish of diameter 90 mm (not shown in the figure). The deformation of the water surface is created by the movable Teflon barrier (2). The barrier is 88 mm wide and its lower edge is carefully

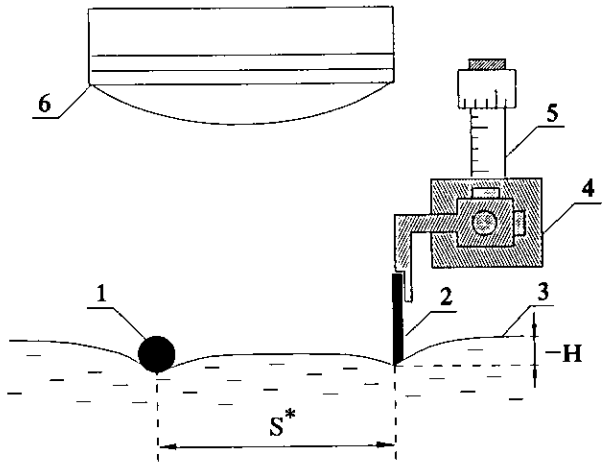

FIG. 1. Experimental setup for measurement of the equilibrium position of a floating particle in the neighborhood of a wall: (1) spherical particle, (2) movable Teflon barrier, (3) water surface, (4) micrometric table, (5) precise micrometric screw, (6) long focus microscope.

straightened and polished. The alignment of the plate with respect to the water surface is controlled by means of the micrometric table (4) with four degrees of freedom. The vertical movement of the plate in these experiments ought to be very precise in order to create and control the deformation of the surface. A special micrometric screw (5) with a precision of ± 0.6 μm has been used for that purpose. It allows accurate measurement of the changes in the depth of plate immersion, H (Fig. 1), but not of the absolute value of H itself. The unknown additive constant is determined by means of the least-squares method when the data are fit for H—see Section 4 below.

For each given depth of immersion, H, the floating particle rests in an equilibrium position at some distance, s^*, from the wall. In this position the capillary image force, repelling the particle from the wall, is exactly counterbalanced by the gravity force (including the upthrust). The measurement of the distance, s^*, between the plate and the floating particle is carried out by means of a wide-view, long-focus microscope (Citoval 2, Carl Zeiss, Jena) situated above the dish with the liquid. The precision of measurement of s^* is better than ± 20 μm.

In order to determine the three-phase contact angle we observed the position of the floating particle (copper bead or mercury drop) in a spectroscope cuvette ($50 \times 18 \times 30$ mm) partially filled with water. Photographs, like that shown in Fig. 2, are taken through the vertical optical walls of the cuvette. The geometrical parameters characterizing the particle position (equatorial radius, radius of three-phase contact line, and depth of immersion into the water) are measured from the photographs by means of optical densitometer and are used for calculation of the contact angle.

The temperature was kept at 25 ± 0.5°C during the experiments.

FIG. 2. Photograph of the immersed part of a mercury drop floating attached to a water–air interface. From the equatorial radius and the depth of immersion of the drop one can calculate precisely the three-phase contact angle.

3. DETERMINATION OF THE THREE-PHASE CONTACT ANGLE α_2

(a) Determination of α_2 for Spherical Particles

The contact angle at which the water surface meets the particle surface is an important parameter for the capillary interaction. We assume that the interfacial tension, γ, the mass densities of the two fluid phases, ρ_{I} and ρ_{II}, and that of the particle, ρ_2, are known. From the photographs we measure the particle radius, R_2, the radius of the three-phase contact line, r_2, and the depth of immersion into the lower phase, b_2 (see Fig. 3). Then one can use either the values of R_2 and b_2 or the values of R_2 and r_2 to calculate α_2 and the meniscus slope angle ψ_2 by using a simple iterative procedure. If the pair of parameters R_2 and b_2 is known, the procedure is the following:

(i) r_2 and the part of the particle volume which is immersed in the lower phase, V_l, are calculated from the geometrical relationships

$$r_2 = [b_2(2R_2 - b_2)]^{1/2} \qquad [3.1]$$

$$V_l = \pi b_2^2(R_2 - b_2/3). \qquad [3.2]$$

(ii) An initial value for the meniscus slope angle at the three-phase contact line, $\psi_2^{(0)}$, is prescribed; we use $\psi_2^{(0)} = 0$.

(iii) The subsequent approximation for the capillary charge, Q_2, is calculated from the equation

$$Q_2^{(k+1)} = r_2 \sin \psi_2^{(k)}. \qquad [3.3]$$

(iv) The next approximation for the particle contact line elevation, h_2, is determined from a counterpart of Derjaguin's formula (14),

$$h_2^{(k+1)} = Q_2^{(k+1)} \ln\{4/[\gamma_e q r_2(1 + \cos \psi_2^{(k)})]\}, \qquad [3.4]$$

where $\gamma_e = 1.781071\ldots$ is the constant of Euler–Masceroni,

$$q^2 = (\rho_{\mathrm{I}} - \rho_{\mathrm{II}})g/\gamma, \qquad [3.5]$$

g is the gravity acceleration, and γ is the surface tension of water.

(v) The next approximation for ψ_2 is obtained from the vertical force balance (see Refs. (6, 15))

$$\psi_2^{(k+1)} = \arcsin\left[\frac{q^2}{2\pi r_2}\left(V_l - \frac{4}{3}\pi D_2 R_2^3 - \pi r_2^2 h_2^{(k+1)}\right)\right], \qquad [3.6]$$

where

$$D_2 = (\rho_2 - \rho_{\mathrm{II}})/(\rho_{\mathrm{I}} - \rho_{\mathrm{II}}). \qquad [3.7]$$

(vi) If $|1 - \psi_2^{(k)}/\psi_2^{(k+1)}| \geq \epsilon$ the iteration process is repeated from point (iii). Here ϵ is the relative error which was fixed in advance. We used $\epsilon = 10^{-8}$.

(vii) Finally α_2 is determined from the geometrical relationship

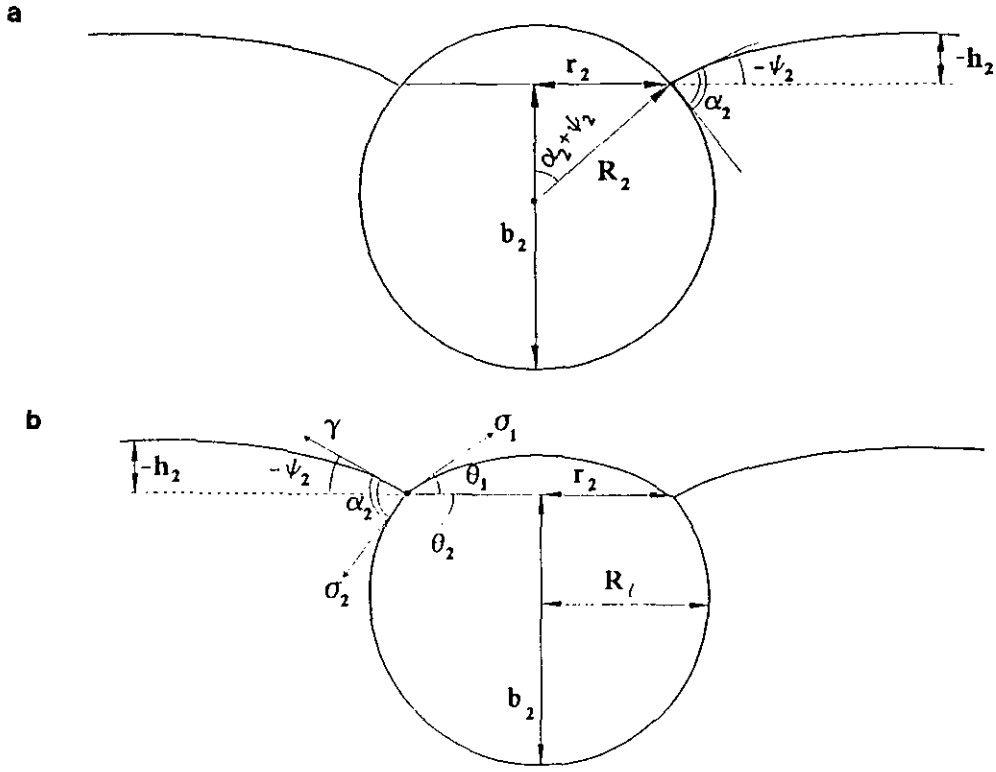

FIG. 3. Sketch of a spherical solid particle (a) and a mercury drop (b) attached to a fluid interface.

$$\alpha_2 = \arcsin(r_2/R_2) - \psi_2^{(k+1)}. \qquad [3.8]$$

Our computational experience showed that this procedure is rapidly convergent and it is not very sensitive to the choice of the initial value $\psi_2^{(0)}$.

If the pair of parameters R_2 and r_2 is known, the iterative procedure is the same with the exception of step (i), in which b_2 is calculated from the equation

$$b_2 = R_2 + (R_2^2 - r_2^2)^{1/2}\text{sign}(b_2 - R_2), \qquad [3.9]$$

where sign $(b_2 - R_2)$ equals 1 or -1 depending on whether the contact line is above or below the particle equator.

The use of the pair of parameters R_2 and b_2 is preferable for particles with contact angle α_2 close to 90°, because it gives more accurate results (small variation in α_2 leads to a large change in b_2).

(b) Determination of α_2 for Mercury Drops

For mercury drops the procedure for calculating α_2 should be slightly modified, because their shape is not a perfect sphere but is composed of spherical segments—see Fig. 3b. This is due to the fact that the mercury–air surface tension, σ_1, is greater than the mercury–water interfacial tension, σ_2. (The deformation of the drop due to gravity is negligible because of the high interfacial tensions—see, e.g., Ref. (15)). The radii of curvature of these spherical surfaces are determined from the ratio of the interfacial tensions σ_1 and σ_2. In our computations we assume that $\sigma_2 = 426$ mN/m (16) and $\gamma = 72$ mN/m. The radius of curvature of the mercury–water interface, R_l, and the depth of immersion, b_2, are measured from the photographs (cf. Figs. 2 and 3b). Then the three-phase contact angle, α_2, the meniscus slope angle, ψ_2, and σ_1 are determined by means of the following iterative procedure:

(i) From R_l and b_2 we calculate

$$r_2 = [b_2(2R_l - b_2)]^{1/2} \qquad [3.10]$$

$$V_l = \pi b_2^2(R_l - b_2/3) \qquad [3.11]$$

$$\theta_2 = \pi - \arcsin(r_2/R_l). \qquad [3.12]$$

(ii) An initial approximation for $\psi_2^{(0)}$ is given; we use $\psi_2^{(0)} = 0$.

(iii) The subsequent approximations for α_2 and Q_2 are calculated from the expressions

$$\alpha_2^{(k+1)} = \pi - \theta_2 - \psi_2^{(k)} \qquad [3.13]$$

$$Q_2^{(k+1)} = r_2 \sin \psi_2^{(k)}. \qquad [3.14]$$

(iv) From Neumann–Young triangle and geometrical considerations one can calculate

$$\sigma_1^{(k+1)} = (\sigma_2^2 + \gamma^2 + 2\gamma\sigma_2\cos\alpha_2^{(k+1)})^{1/2} \quad [3.15]$$

$$\theta_1^{(k+1)} = \arccos[(\gamma\cos\psi_2^{(k)} - \sigma_2\cos\theta_2)/\sigma_1^{(k+1)}] \quad [3.16]$$

$$R_u^{(k+1)} = r_2/\sin\theta_1^{(k+1)} \quad [3.17]$$

$$V_u^{(k+1)} = (\pi/3)(R_u^{(k+1)})^3 \times [1 - \cos\theta_1^{(k+1)}]^2[2 + \cos\theta_1^{(k+1)}], \quad [3.18]$$

where R_u is the radius of curvature of the drop cap.

(v) $h_2^{(k+1)}$ is determined from Derjaguin's formula—see Eq. [3.4].

(vi) The subsequent approximation for ψ_2 is calculated from the vertical force balance

$$\psi_2^{(k+1)} = \arcsin\left[\frac{q^2}{2\pi r_2}(V_l - D_2(V_l + V_u^{(k+1)}) - \pi r_2^2 h_2^{(k+1)})\right]. \quad [3.19]$$

(vii) If $|1 - \psi_2^{(k)}/\psi_2^{(k+1)}| \geqslant \epsilon$ the iteration process is repeated from point (iii). Here ϵ is the relative error which is fixed in advance. Our calculations showed that this procedure is quickly convergent.

4. CALCULATION OF THE THEORETICAL DEPENDENCE $H(s^*)$

In the first part of this study we derived an expression for the lateral capillary force, F_t, between the floating particle and the wall—see Eqs. [5.6]–[5.8], [5.16], and [5.17] in Ref. (13). At equilibrium $F_t = 0$. For a fixed contact line at the wall surface (which is the case in our experiments) the deformation of the water surface, ζ_1, created by the wall is given by Eq. [3.8] in Ref. (13). Then the condition for equilibrium separation s^* at a given H can be written in the form

$$(\gamma/r_2)Y(s^*, H) - 2\pi\gamma Q_2 Hq\exp(-qs^*) = 0, \quad [4.1]$$

where

$$Y(s^*, H) = \int_0^\pi [2Q_2\zeta_0(\varphi) + (d\zeta_0/d\varphi)^2 + q^2r_2^2\zeta(\varphi)^2]\cos\varphi d\varphi, \quad [4.2]$$

where $\zeta_0(\varphi)$ and $\zeta(\varphi) = \zeta_0(\varphi) + \zeta_1(\varphi)$ are given by Eqs. [3.8], [3.29], and [5.9] in Ref. (13). Hence Eq. [4.1] is a transcendental equation which connects H and s^*.

To solve Eq. [4.1] and to find H at given s^* we used the following iterative procedure:

(i) The parameters of the system (fluid and particle mass densities, particle size and contact angle, interfacial tension) are considered to be known.

(ii) An initial approximation $H^{(0)}$ is taken (we used $H^{(0)} = 0$).

(iii) At given $H^{(k)}$ ($k = 0, 1, 2, 3, \cdots$) we calculate the other geometrical quantities $r_2^{(k)}$, $b_2^{(k)}$, $Q_2^{(k)}$, and $\psi_2^{(k)}$ from the normal balance of the gravity, buoyancy, and surface tension forces—see Section 3d in Ref. (13). For that reason, the iterative procedure described in Section 6a of Ref. (13) is applied.

(iv) By using the parameters obtained in point (iii), the next approximation for H is determined from a counterpart of Eq. [4.1]:

$$H^{(k+1)} = Y(s^*, H^{(k)})\exp(qs^*)/(2\pi q r_2^{(k)} Q_2^{(k)}). \quad [4.3]$$

(v) If $|1 - H^{(k)}/H^{(k+1)}| \geqslant \epsilon$ the iteration process is repeated from point (iii); ϵ is the relative error of the calculations (we use $\epsilon = 10^{-8}$).

This procedure converges very fast. For the *mercury drops* it was modified in order to account for the fact that their shape is not perfectly spherical. The respective procedure is described in the Appendix and is used in step (iii) instead of the procedure for *spherical particles.*

The computations showed that the calculated dependence $H(s^*)$ is very sensitive to the particle radius but is slightly dependent on α_2 for the particles studied experimentally. Thus, for comparison of the theory and the experiment, we adopt the following procedure. The contact angle α_2 is measured as described in Section 3 and is considered as a fixed parameter for the given type of particles. The particle radius R_2 (or R_l for mercury drops) is determined by optical microscopy. Finally, the correctness and self-consistency of the theory are verified by simulation of the experimental data with the theoretical curve $H(s^*)$ at the values of α_2 and R_2 (or R_l) determined in advance.

The calculations showed that the variations of R_2 (R_l) and α_2, within the limits of the experimental accuracy, practically do not affect the calculated values of H at a given separation, s^*, when $qs^* \geqslant 1.5$ (for the particles studied). For that reason we determined the unknown additive constant in the experimental data for H by fitting the last four or five experimental points (these with $qs^* \geqslant 1.5$) with the theoretical curve.

5. EXPERIMENTAL RESULTS AND DISCUSSION

(a) The Three-Phase Contact Angle

For determination of the three-phase contact angle we took pictures of the particles as described in Section 2. Figure 2 presents a photograph of a mercury drop and the water meniscus surrounding it. Due to the drop weight the water surface is curved and the upper part of the drop (which is inside the air phase) cannot be seen in the photograph. From this photograph we measured $R_l = 423.5 \pm 2$ μm, $b_2 = 542$

$\pm$ 5 μm, and r_2 = 406.5 $\pm$ 1 μm. Following the procedure described in Section 3b, from the values of R_l, b_2, and σ_2 we calculated r_2 = 406.6 μm, α_2 = 85.3°, and σ_1 = 438 mN/m. The agreement between the measured and calculated values of r_2 confirms the sphericity of the mercury–water interface. The value of σ_1 determined in this way is lower than the values of the surface tension of mercury, about 470–484 mN/m, quoted in the literature (16, 17). We believe that in our experiments the surface tension of the mercury–air surface is reduced due to the absorption of water from the gaseous phase (17). The literature values are measured with mercury in contact with dry atmosphere saturated with only mercury vapors. Since there is some uncertainty about the precise value of the mercury–water interfacial tension, σ_2 we performed the calculations for the same drop by imposing some lower value of σ_2, say σ_2 = 415 mN/m (17), instead of σ_2 = 426 mN/m (16). The calculated values of r_2, α_2, and ψ_2 were exactly the same. Only for the mercury–air interfacial tension was a different value, σ_1 = 427 mN/m, obtained. This means that the drop shape and the other geometrical parameters, α_2 and ψ_2, slightly depend on the prescribed value of σ_2. Hence we do not claim that the values of σ_1 and σ_2 are exact. However, in spite of that the geometrical parameters and especially the contact angle, α_2, are determined correctly. In principle σ_1 and σ_2 can be determined from some other method (e.g., pendent drop method) but this is beyond the purpose of our study.

It should be noted that the calculated meniscus slope angle at the three-phase contact line, $\psi_2 = -11.5° \pm 0.1°$, is small enough to justify the usage of the linearized Laplace equation of capillarity in our theoretical treatment (the expressions for ζ and ζ_1 used in Eq. [4.2] are derived in Part I (13) for $\sin^2\psi_2 \ll 1$).

For a mercury drop of bigger size we measured R_l = 518 $\pm$ 3 μm, r_2 = 484 $\pm$ 5 μm, and b_2 = 701 $\pm$ 10 μm. Then we calculated α_2 = 87.1° $\pm$ 1° and $\psi_2 = -17.8° \pm 0.2°$. The numerical simulations show that the curves $H(s^*)$ are weakly sensitive to the exact value of α_2 for the particles investigated in our experiments. Thus the variation of α_2 within $\pm 5°$ practically does not change the theoretical curves in the limits of the experimental error. That is why we used for mercury in the computations below the mean value of the aforementioned two experiments, α_2 = 86°.

Similarly, we measured the contact angle of the copper beads to lie between 95° and 105° for different particles. This larger scattering is due to the hysteresis of the contact angle at the solid surface, which is not perfectly smooth and homogeneous. The large values of the contact angle indicate high hydrophobicity of the beads, which is an indication that they are covered with a protecting organic solid film (by the producer). When calculating the theoretical curve, shown dashed in Fig. 4, we used the mean value α_2 = 100°.

As an illustration we present the results for one of the investigated copper beads. From optical measurement we

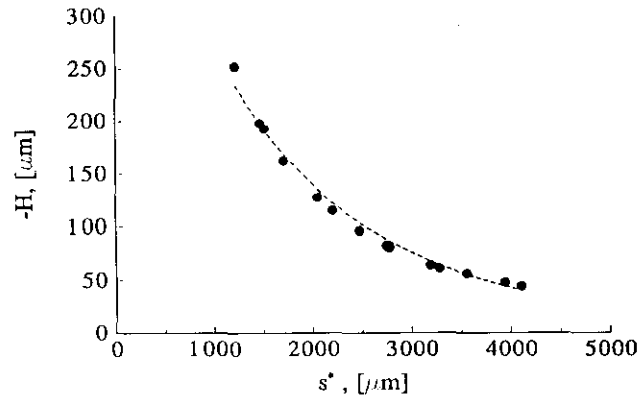

FIG. 4. Experimental data (the circles) for H vs s^* for a copper bead. The theoretical dashed curve is calculated with α_2 = 100° (measured as explained in Section 3a) and R_2 = 700 $\pm$ 10 μm, measured independently by microscope.

determined R_2 = 612 $\pm$ 5 μm, r_2 = 600 $\pm$ 5 μm, and b_2 = 728 $\pm$ 5 μm. Following the procedures described in Section 3a we calculated from the pair R_2 and b_2 the values α_2 = 95.1°, r_2 = 601 μm, and $\psi_2 = -16.0°$. From the values of R_2 and r_2 we calculated α_2 = 94.7°, b_2 = 733 μm, and $\psi_2 = -16.0°$. As seen from these figures the agreement between the measured and calculated values of r_2 and b_2 is very good, which confirms the reliability of the method.

(b) Capillary Image Force

As described above we measured the equilibrium distance, s^*, between the particle center and the wall surface as a function of the height of the lower edge of the hydrophobic Teflon plate, H, where H is evaluated with respect to the level of the horizontal flat interface far from the plate and the particle.

In Fig. 4 the experimental results (the circles) for a copper bead are shown. The respective theoretical curve (see the previous section for the method of its calculation) is also plotted. The values of the three-phase contact angle α_2 = 100° and the particle radius R_2 = 700 $\pm$ 10 μm, used in the calculations, were determined by optical microscopy. As mentioned earlier the variation of the contact angle α_2 with $\pm 5°$ practically does not change the shape of the theoretical curve. This low sensitivity with respect to the value of α_2 does not allow the plot of H vs s^* to be used as a method for determining α_2.

The experimental data show that the larger the magnitude of H (i.e., the larger the surface deformation created by the wall), the smaller the equilibrium separation. One should note that s^* cannot be smaller than the radius of the floating particle, because the distance $s^* = R_2$ corresponds to a direct contact between the particle and the wall.

Figure 5 shows the results for two mercury drops of different size: R_2 = 440 $\pm$ 10 μm (the circles) and R_1 = 512 $\pm$ 10 μm (the boxes). Contact angle α_2 = 86° is used in these

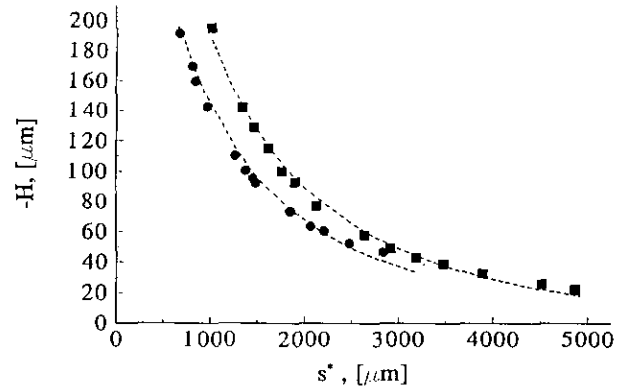

FIG. 5. Experimental results for H versus s^* for two mercury drops of different size. The theoretical curves (dashed) are calculated with $\alpha_2 = 86°$ (measured as described in Section 3b), and $R_l = 440 \pm 10$ μm (lower curve) and $R_l = 512 \pm 10$ μm (upper curve), respectively, measured by optical microscopy.

calculations. Although in this case the particles are fluid, the shape of the curves $H(s^*)$ is very similar to that for the solid copper beads (Fig. 4).

The accuracy and reproducibility of the measurements are about ±2 μm for H and ±20 μm for s^*. As seen from the figures the agreement between the theoretical curve and the experimental points is very good. It is worthwhile to note that, except for the additive constant in the data for H, discussed at the end of Section 4, the theoretical curves in Figs. 4 and 5 are drawn without using any other adjustable parameter.

At the equilibrium position, $s = s^*$, the pure capillary image force, F_C, is exactly counterbalanced by the gravity force (weight plus upthrust), F_G. In other words,

$$F_t(s^*) = F_C(s^*) + F_G(s^*) = 0. \qquad [5.1]$$

As explained in Part I (13), the pure capillary image force can be expressed by setting $H = 0$ in Eq. [5.6] in Ref. (13):

$$F_C(s) = F_t(s, H = 0) = \frac{\gamma}{r_2}\int_0^{\pi} d\varphi \cos\varphi\left[2Q_2\zeta_0(\varphi) + \left(\frac{d\zeta_0}{d\varphi}\right)^2 + q^2r_2^2\zeta_0^2(\varphi)\right] \qquad [5.2]$$

(see also Eqs. [2.1], [5.8], [5.16], and [5.17] in Ref. (13)). Equation [5.2] allows one to determine F_C for the systems studied. As an illustration, the plot of F_C vs s^* for the two mercury drops (cf. Fig. 5) is shown in Fig. 6. It is seen from Fig. 6 that the magnitude of the capillary image force is on the order of 10^{-6} N for the particles studied.

6. CONCLUSIONS

In this article we investigate experimentally the capillary meniscus interaction between a floating spherical particle and a vertical wall (see Fig. 1). The existence of an equilibrium particle–wall separation, s^*, predicted in Part I (13), was proven experimentally. The separation, s^*, was measured as a function of the wall immersion, H. The experimental plots of H vs s^* are compared with the theory developed in the first part of this study (13)—see Figs. 4 and 5. The agreement between the theory and experiment is very good. A simple method for determination of the three-phase contact angle of millimeter- and submillimeter-size floating particles is described.

APPENDIX

Determination of the Geometrical Parameters of a Floating Mercury Drop Used in the Calculation of $H(s^*)$

As mentioned earlier, the shape of the mercury drops is not spherical due to the difference between the interfacial tensions σ_1 and σ_2 (see Fig. 3b). For that reason, the procedure for determining the geometry of mercury drops floating attached to a liquid interface in the vicinity of a wall is different from that in the case of solid spherical particles, described in Section 6a in Ref. (13)—see also Section 3b in this study.

Let us assume that we have determined the contact angle, α_2, and the interfacial tensions, σ_1 and σ_2, of the mercury drop. In addition, the initial drop radius, R_0 (without deviation from sphericity), the mass density ratio, D_2, the surface tension, γ, and the capillary length, q^{-1}, are also known. In order to determine the drop capillary charge, Q_2, as well as the contact line radius, r_2, we use the following iterative procedure:

(i) The procedure starts with the choice of an initial guess for ψ_2 and r_2,

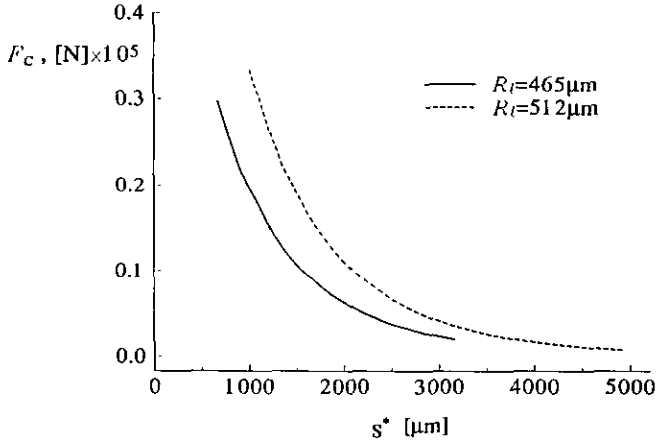

FIG. 6. Plot of the pure capillary image force, F_C vs s^*, (calculated from Eq. [5.2]) for the same mercury drops, as in Fig. 5.

$$\psi_2^{(0)} = 0, \quad r_2^{(0)} = R_0 \sin \alpha_2. \qquad [A.1]$$

(ii) The next approximation for θ_2 is calculated from the geometrical relationship

$$\theta_2^{(k+1)} = \pi - \alpha_2 - \psi_2^{(k)}. \qquad [A.2]$$

(iii) $\theta_1^{(k+1)}$ is calculated from Eq. [3.16], where $\theta_2 = \theta_2^{(k+1)}$.

(iv) The next approximation for r_2 is calculated from the balance of the drop volume,

$$r_2^{(k+1)} = R_0 \left[\frac{(1 - \cos \theta_1^{(k+1)})^2 (2 + \cos \theta_1^{(k+1)})}{\sin^3 \theta_1^{(k+1)}} + \frac{(1 - \cos \theta_2^{(k+1)})^2 (2 + \cos \theta_2^{(k+1)})}{\sin^3 \theta_2^{(k+1)}} \right]^{-1/3}. \qquad [A.3]$$

(v) The volume of the drop situated below the contact line, V_l, is determined from the relationship

$$V_l^{(k+1)} = \frac{\pi}{3} \left(\frac{r_2^{(k+1)}}{\sin \theta_2^{(k+1)}} \right)^3 \times (1 - \cos \theta_2^{(k+1)})^2 (2 + \cos \theta_2^{(k+1)}). \qquad [A.4]$$

(vi) $Q_2^{(k+1)}$ is calculated from Eq. [3.3] with $r_2 = r_2^{(k+1)}$.

(vii) $h_2^{(k+1)}$ is calculated from Eq. [3.42] in Ref. (13).

(viii) The next approximation for ψ_2 is determined

$$\psi_2^{(k+1)} = \arcsin \left[\frac{q^2}{2\pi r_2^{(k+1)}} \left(V_l^{(k+1)} - \frac{4}{3} \pi R_0^3 D_2 - \pi (r_2^{(k+1)})^2 h_2^{(k+1)} \right) \right]. \qquad [A.5]$$

(ix) if $|1 - Q_2^{(k)}/Q_2^{(k+1)}| < \epsilon$ the iteration process stops, otherwise, the next iteration repeats from step (ii) ϵ is the relative error of the calculations.

ACKNOWLEDGMENT

This work was supported by Nagayama Protein Array Project under the Program "Exploratory Research for Advanced Technology" (ERATO) of the Research and Development Corporation of Japan (JRDC).

REFERENCES

1. Nicolson, M. M., *Proc. Cambridge Philos. Soc.* **45,** 288 (1949).
2. Gifford, W. A., and Scriven, L. E., *Chem. Eng. Sci.* **26,** 287 (1971).
3. Chan, D. Y. C., Henry, J. D., and White, L. R., *J. Colloid Interface Sci.* **79,** 410 (1981).
4. Kralchevsky, P. A., Paunov, V. N., Ivanov, I. B., and Nagayama, K., *J. Colloid Interface Sci.* **151,** 79 (1992).
5. Kralchevsky, P. A., Paunov, V. N., Denkov, N. D., Ivanov, I. B., and Nagayama, K., *J. Colloid Interface Sci.* **155,** 420 (1993).
6. Paunov, V. N., Kralchevsky, P. A., Denkov, N. D., and Nagayama, K., *J. Colloid Interface Sci.* **157,** 100 (1993).
7. Paunov, V. N., Kralchevsky, P. A., Denkov, N. D., Ivanov, I. B., and Nagayama, K., *Colloids Surf.* **67,** 119 (1992).
8. Kralchevsky, P. A., and Nagayama, K., *Langmuir* **10,** 23 (1994).
9. Allain, C., and Cloitre, M., *J. Colloid Interface Sci.* **157,** 261 (1993).
10. Allain, C., and Cloitre, M., *J. Colloid Interface Sci.* **157,** 269 (1993).
11. Velev, O. D., Denkov, N. D., Kralchevsky, P. A., Paunov, V. N., and Nagayama, K., *Langmuir* **9,** 3702 (1993).
12. Camoin, C., Roussel, J. F., Faure, R., and Blanc, R., *Europhys. Lett.* **3,** 449 (1987).
13. Kralchevsky, P. A., Paunov, V. N., Denkov, N. D., and Nagayama, K., *J. Colloid Interface Sci.* **166,** 47 (1994).
14. Derjaguin, B. V., *Dokl. Akad. Nauk USSR* **51,** 517 (1946).
15. Kralchevsky, P. A., Nikolov, A. N., and Ivanov, I. B., *J. Colloid Interface Sci.* **112,** 108 (1986).
16. Jaycock, M. J., and Parfitt, G. D., "Chemistry of Interfaces." Wiley, New York, 1981.
17. Adamson, A. W., "Physical Chemistry of Surfaces," third ed. Wiley, New York, 1976.